

Five mononuclear pentacoordinate Co(II) complexes with field-induced slow magnetic relaxation



Cyril Rajnák^{a,c,d,*}, Ján Titiš^a, Jozef Miklovič^a, George E. Kostakis^b, Olaf Fuhr^c, Mario Ruben^{c,d}, Roman Boča^a

^a Department of Chemistry, FPV, University of SS Cyril and Methodius, 91701 Trnava, Slovakia

^b Department of Chemistry, School of Life Sciences, University of Sussex, Brighton BN1 9QJ, United Kingdom

^c Institute of Nanotechnology, Karlsruhe Institute of Technology (KIT), Postfach 3640, 76021, Germany

^d IPCMS-CNRS, Université de Strasbourg, 23, rue du Loess, F-67034 Strasbourg, France

ARTICLE INFO

Article history:

Received 4 November 2016

Accepted 18 January 2017

Available online 28 January 2017

Keywords:

Crystal structure

Magnetic data

Co(II) complexes

Field-induced slow magnetic relaxation

Pentacoordination

ABSTRACT

Five related mononuclear pentacoordinate complexes of the formula $[\text{CoL}^n\text{Cl}_2]$ show slow magnetic relaxation under small applied DC field; L^3 – a tridentate N-donor ligand based upon dipyrazolpyridine with an alkyl tail. All of them exhibit a supramolecular assembly, either forming dimers or chains *via* π – π stacking. Moreover, they display two relaxation branches, one being typical for single molecule magnets of this class, $\tau \sim 10^{-6}$ s, and the second one as slow as $\tau \sim 0.5$ s at $T = 1.9$ K.

© 2017 Elsevier Ltd. All rights reserved.

1. Introduction

The family of single-molecule magnets (SMM) based upon mononuclear Co(II) complexes is rapidly growing in recent years [1]. They cover octacoordinate, heptacoordinate, hexacoordinate, pentacoordinate, tetracoordinate, as well as tricoordinate complexes [2–7]. While the hexacoordinate complexes are quasi-octahedral and the tetracoordinate ones quasi-tetrahedral, the pentacoordinate complexes could adopt either square-pyramidal or trigonal-bipyramidal geometry, and more often their geometry is in between these limiting cases. The barrier to spin reversal for these complexes spans typically the range $U/k_B = 10$ –40 K (except hexacoordinate complexes) and the extrapolated relaxation time is $\tau_0 = 10^{-6}$ – 10^{-10} s. However, these data were extracted from a simple (linear) Arrhenius equation for $\ln\tau$ vs $1/T$ that holds true for the pure thermally activated Orbach process applicable to the higher temperature region. More complex analysis, that simultaneously includes the direct, Raman, and Orbach processes is appearing [8]; however, the interrelation to the “older” U – τ_0 data set was not reported so far so that the reliability of those old data is unknown.

Recently, one pentacoordinate Co(II) complex supported by antenna-like ligand has been assigned as a field induced SMM with $U/k_B = 13.5$ K and $\tau_0 = 1.35 \times 10^{-7}$ s for the faster of two observed relaxation branches [5c]. This complex, $[\text{CoCl}_2\text{L}^{C7}]_2$, is a member of the related complexes with shorter or longer antenna-like aliphatic chains: L^{C7} abbreviates 4-hept-1-ynyl-2,6-di-pyrazol-1-yl-pyridine. Two members of this family (for L^{C0} and L^{C12}) have been described and characterized in the past with DC magnetic data matching mononuclear Co(II) systems with large magnetic anisotropy ($D/hc \sim 71$ and 47 cm^{-1} , respectively) [9]. The AC susceptibility measurements were not conducted that time. Herein we are reporting about synthesis, characterization and X-ray structure of other two complexes using L^{C10} and L^{C14} ligands, along with the AC susceptibility data for all five members of the mentioned family. The ligands L^{Cn} are sketched in Scheme 1; their complexes are abbreviated **1** through **5** following the length of the alkyl chain.

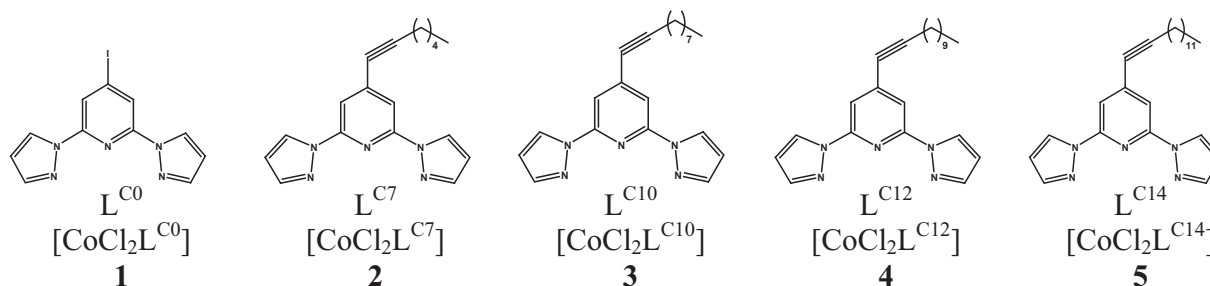
2. Experimental

2.1. Chemicals and handling

All chemicals in this study were purchased from Sigma–Aldrich and Merck and used as received. The solvents, *n*-hexane, EtOAc, were used without further purification; CH_3CN and $(^1\text{Pr})_2\text{NH}$ were dried by distillation over CaH_2 .

* Corresponding author at: Department of Chemistry, FPV, University of SS Cyril and Methodius, 91701 Trnava, Slovakia.

E-mail address: rajnak.cyril@gmail.com (C. Rajnák).



Scheme 1. Sketch of the tridentate ligands, their abbreviations and complexes. Systematic names: L^{C0} = 4-iodo-2,6-di-pyrazol-1-yl-pyridine; L^{C7} = 4-hept-1-ynyl-2,6-di-pyrazol-1-yl-pyridine; L^{C10} = 4-dec-1-ynyl-2,6-di-pyrazol-1-yl-pyridine; L^{C12} = 4-dodec-1-ynyl-2,6-di-pyrazol-1-yl-pyridine; L^{C14} = 4-tetradec-1-ynyl-2,6-di-pyrazol-1-yl-pyridine.

2.2. Physical measurements

^1H and ^{13}C NMR spectra were recorded using FT-NMR Spectrometer (Avance III 500 MHz, Bruker) with solvent proton ($\text{CDCl}_3\text{-d}_1$, 99.8 atom% D) as an internal standard. The solid KBr for FT-IR measurements was kept against absorption of moisture in an oven at 60°C , prior to the using. The infrared spectra in KBr pellets in the range $4000\text{--}400\text{ cm}^{-1}$ were acquired at room temperature using by FT-IR spectrometer (Spectrum GX, Perkin Elmer). Electronic spectra were measured by UV-Vis-NIR spectrophotometer (Cary 500 Scan, Varian and Specord 250 Plus, Analytica Jena with DAD detector) in mineral oil suspension (Nujol) and MeCN (HPLC grade $\geq 99.93\%$) as a solvent. Mass spectra were measured by electrospray ionization time of flight technique on microTOF-QII for ESI-TOF (Bruker) and data were taken in the positive mode of ion polarity. Samples for ESI-TOF were dissolved in a few amount of dry acetonitrile. Elemental analyses were carried out on a Vario MICRO cube. For thin-layer chromatography a polyester sheets POLYGRAM ALOX N/UV₂₅₄ with 0.2 mm thickness of aluminium oxide layer were used under the ultraviolet light. Melting points were determined Melting Point B-540 (Büchi).

2.3. Preparation of ligands and complexes

The 4-iodo-2,6-di-pyrazol-1-yl-pyridine, L^{C0} , was synthesized following reported procedures [10]. The remaining ligands were synthesized according to the Scheme 2.

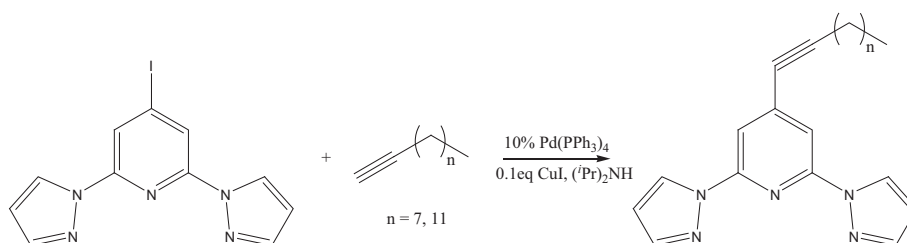
2.3.1. Preparation of 4-tetradec-1-ynyl-2,6-di-pyrazol-1-yl-pyridine (L^{C14})

In a 100 cm^3 two necked round bottom flask, a freshly distilled solvent (^iPr)₂NH (60 cm^3) was deoxygenated under the Ar flux for 1 h. 4-iodo-2,6-di-pyrazol-1-yl-pyridine (0.674 g, 2 mmol), 10% of $\text{Pd}^0(\text{PPh}_3)_4$ and CuI (0.038 g, 0.2 mmol) were suspended in an Ar-gas bubbled solution of (^iPr)₂NH and stirred for 1 h. 1-tetradecyne (0.777 g, 4 mmol) was added and the mixture was stirred for 4 days at ambient temperature. The solvent was removed using a rotary evaporator. The solid residue was at first column chro-

matographed on aluminium oxide (activated neutral) with EtOAc/*n*-Hex (1:20, $R_f = 0.61$) as an eluent. The combined slightly yellowish solutions yielded upon evaporation and dried in vacuum to 0.32 g of a white powder (0.79 mmol, 40%). $\text{C}_{25}\text{H}_{33}\text{N}_5\cdot 0.1\text{ CH}_3\text{-OH}\cdot 0.15\text{ Hexane}$: calcd. C 74.41, H 8.53, N 16.69; found C 74.63, H 7.92, N 16.28. ^1H NMR (500 MHz, $\text{CDCl}_3\text{-d}_1$, 21°C) δ (ppm) 8.54 (d, $J = 2.5\text{ Hz}$, 2H), 7.83 (s, 2H), 7.75 (s, 2H), 6.49 (t, $J = 1.75\text{ Hz}$, 2H), 2.45 (t, $J = 7.25\text{ Hz}$, 2H), 1.61 (m, 2H), 1.29 (m, 18H), 0.87 (t, $J = 7\text{ Hz}$, 3H). ^{13}C NMR (125 MHz, CDCl_3) δ (ppm) 150.11, 142.42, 137.73, 127.08, 111.69, 108.01, 97.45, 78.32, 31.92, 29.67, 29.65, 29.51, 29.36, 29.15, 28.91, 28.34, 22.69, 19.51, 14.12. UV-Vis (CH_3CN): λ_{max} (ϵ , $\text{M}^{-1}\text{ cm}^{-1}$) = 250(58772), 322(14254). FT-IR (KBr) ν/cm^{-1} 2915(s), 2851(m), 2243(w), 1615 (s), 1555(s), 1525(m), 1470(s), 1399(s), 1210(m), 1053(m), 959 (m), 857(m), 792(m), 757(s). Mp: $56\text{--}58^\circ\text{C}$. ESI-TOF MS (CH_3CN): $m/z = 404.24\text{ [M]}+\text{H}^+$.

2.3.2. Preparation of 4-dec-1-ynyl-2,6-di-pyrazol-1-yl-pyridine (L^{C10})

In a 100 cm^3 two necked round bottom flask, a freshly distilled (^iPr)₂NH (60 cm^3) as the solvent was deoxygenated under the Ar flux for 1 h. 4-iodo-2,6-di-pyrazol-1-yl-pyridine (0.674 g, 2 mmol), 10% of $\text{Pd}^0(\text{PPh}_3)_4$ and CuI (0.038 g, 0.2 mmol) were suspended in an Ar-gas bubbled solution of (^iPr)₂NH and stirred for 1 h. 1-Decyne (0.553 g, 4 mmol) was added and the mixture was stirred for 4 days at ambient temperature. The solvent was removed using a rotary evaporator. The solid residue was at first column chromatographed on aluminium oxide (activated, neutral) with EtOAc/*n*-Hex (1:20, $R_f = 0.46$) as an eluent. The combined slightly yellowish solutions yielded upon evaporation and dried in vacuum to 0.41 g of a white powder (1.18 mmol, 59%). $\text{C}_{21}\text{H}_{25}\text{N}_5\cdot 0.3\text{ CH}_3\text{-OH}\cdot 0.05\text{ Hexane}$: calcd. C 71.79, H 7.50, N 19.38; found C 71.70, H 7.02, N 18.85. ^1H NMR (500 MHz, $\text{CDCl}_3\text{-d}_1$, 21°C) δ (ppm) 8.53 (d, $J = 2.5\text{ Hz}$, 2H), 7.83 (s, 2H), 7.75 (d, $J = 1\text{ Hz}$, 2H), 6.49 (q, $J = 2\text{ Hz}$, 2H), 2.45 (t, $J = 7\text{ Hz}$, 2H), 1.62 (m, 2H), 1.45 (m, 2H), 1.31 (m, 8H), 0.89 (t, $J = 6.75\text{ Hz}$, 3H). ^{13}C NMR (125 MHz, CDCl_3 , 21°C) δ (ppm) 150.10, 142.43, 137.72, 127.09, 111.69, 108.02, 97.45, 78.32, 31.87, 29.19, 29.13, 28.93, 28.35, 22.68, 19.52, 14.12. UV-Vis (CH_3CN): λ_{max} (ϵ , $\text{M}^{-1}\text{ cm}^{-1}$) = 250(52578), 322



Scheme 2. Synthetic route for preparation of long alkyl chains on 2,6-di-pyrazol-1-yl-pyridine frame via cross-coupling Sonogashira reaction to sp carbon atoms.

(12220). FT-IR (KBr) ν/cm^{-1} 2948(m), 2851(m), 2236(w), 1611(s), 1552(s), 1525(m), 1465(s), 1397(s), 1207(m), 1040(m), 956(m), 936(m), 864(m), 791(m), 763(s). Mp: 42–44 °C. ESI-TOF MS (CH_3CN): $m/z = 348.19$ $[\text{M}]^+\text{H}^+$.

2.3.3. Preparation of $[\text{CoCl}_2\text{L}^{\text{C10}}]$, **3**

In a 100 cm^3 two necked round bottom flask a solution of **L^{C10}** (120 mg, 0.35 mmol) and $\text{CoCl}_2 \cdot 6\text{H}_2\text{O}$ (82.17 mg, 0.35 mmol) in CH_3CN (50 cm^3) was heated at 80 °C for overnight under inert Ar flow. The reaction mixture was cooled down and most of solvent was removed using a rotary evaporator. Yield (blue needles) 130 mg (0.272 mmol, 79%). $\text{C}_{21}\text{H}_{25}\text{CoCl}_2\text{N}_5$: calcd. C 52.84, H 5.28, N 14.67; found C 52.86, H 5.21, N 14.00. Melting point 286–288 °C. ESI-TOF MS (CH_3CN): $m/z = 441.09$ $[\text{M}]^+$. UV-Vis (Nujol): $\nu_{\text{max}}/10^3\text{cm}^{-1}$ (absorbance) = 11.161 (0.083), 16.103 (0.206), 18.832 (0.1614), 24.272 (0.482). UV-VIS (CH_3CN): λ_{max} (ϵ , $\text{M}^{-1}\text{cm}^{-1}$) = 250 (53813), 321 (13380). FT-IR (KBr): $\nu/\text{cm}^{-1} = 3089, 2928, 2855, 2223, 1621, 1567, 1556, 1527, 1497, 1456, 1403, 1336, 1265, 1228, 1049, 968, 764$.

2.3.4. Preparation of $[\text{CoCl}_2\text{L}^{\text{C14}}]$, **5**

In a 100 cm^3 two necked round bottom flask a solution of **L^{C14}** (120 mg, 0.29 mmol) and $\text{CoCl}_2 \cdot 6\text{H}_2\text{O}$ (70.75 mg, 0.29 mmol) in CH_3CN (50 cm^3) was heated at 80 °C for overnight under Ar flow. The reaction mixture was cooled down. Most of solvent was removed using a rotary evaporator. Blue rhomb-shaped crystals were grown by evaporation of CH_3CN solution of the complex at the room temperature in several days. Yield 110 mg (0.206 mmol, 69%). $\text{C}_{25}\text{H}_{33}\text{CoCl}_2\text{N}_5$: calcd. C 56.29, H 6.24, N 13.13; found C 56.42, H 6.11, N 12.53. Melting point 278–279 °C. ESI-TOF MS (CH_3CN): $m/z = 497.15$ $[\text{M}]^+$. UV-Vis (Nujol): $\nu_{\text{max}}/10^3\text{cm}^{-1}$ (absorbance) = 11.601 (0.145), 16.181 (0.412), 18.868 (0.318), 23.866 (0.8714). UV-Vis (CH_3CN): λ_{max} (ϵ , $\text{M}^{-1}\text{cm}^{-1}$) = 250 (58337), 322 (15206). FT-IR (KBr): $\nu/\text{cm}^{-1} = 3086, 2923, 2851, 2233, 1624, 1567, 1498, 1456, 1402, 1335, 1262, 1046, 963, 846, 776$.

2.4. Crystallography

Data for compounds **3** and **5** were collected at 180 K on a Stoe IPDS II area detector diffractometer using graphite-monochromated Mo-K α radiation ($\lambda = 0.71073$ Å).

Semi-empirical absorption corrections were applied using XPREP in SHELXTL and the structures were solved using direct methods, followed by a full-matrix least-squares refinement against F^2 (all data) using SHELXTL [11]. Anisotropic refinement was used for all ordered non-hydrogen atoms; organic hydrogen atoms were placed in calculated positions. The crystal data and the parameters of the structure refinement are listed in Table 1.

2.5. Magnetic data collection

The magnetic data was collected with the SQUID apparatus (MPMS-XL7, Quantum Design) using the RSO mode of detection with ca 30 mg of the sample encapsulated in a gelatine-made sample holder. The DC susceptibility taken at $B_{\text{DC}} = 0.1$ T has been corrected for the underlying diamagnetism. The magnetization has been measured at two temperatures $T = 2.0$ and 4.6 K. The magnetization data was taken in the field-decreasing mode, starting from $B_{\text{DC}} = 7$ T, in order eventually to catch the remnant magnetization. This record is identical with the “virgin” magnetization curve. The AC susceptibility measurements at different frequencies between $f = 0.05$ and 1512 Hz were conducted at oscillating field $B_{\text{AC}} = 0.38$ mT and an applied field $B_{\text{DC}} = 0.2$ T, respectively. Twenty scans were averaged for each measurement; the data outside $|\sigma|$ interval was ignored, the rest was averaged and new standard deviation was calculated for the reduced data set.

Table 1
Crystal data and structure refinement for **3** and **5**.

	Complex 3	Complex 5
Abbr.	$[\text{CoCl}_2\text{L}^{\text{C10}}] \cdot 3\text{CH}_3\text{CN}$	$[\text{CoCl}_2\text{L}^{\text{C14}}]$
Empirical formula	$\text{C}_{27}\text{H}_{34}\text{Cl}_2\text{CoN}_8$	$\text{C}_{25}\text{H}_{33}\text{Cl}_2\text{CoN}_5$
Formula weight/ g mol^{-1}	600.45	533.39
Crystal system	monoclinic	monoclinic
Space group	$P 21/c$	$P 21/c$
T (K)	180(2)	180(2)
Crystal size (mm)	$0.38 \times 0.14 \times 0.05$	$0.20 \times 0.18 \times 0.14$
Z	4	4
a (Å)	13.997(12)	20.261(3)
b (Å)	15.372(9)	8.4397(15)
c (Å)	14.570(10)	15.7328(18)
α (°)	90	90
β (°)	101.679(6)	104.126(9)
γ (°)	90	90
V (Å ³)	3070.0(4)	2608.9(6)
Calculated density D_c / g cm^{-3}	1.299	1.358
Absorption coefficient/ mm^{-1}	0.763	0.885
Reflections collected/ unique	13501/5742 [R(int) = 0.1182]	11319/4445 [R(int) = 0.1528]
Final R indices	$R_1 = 0.0795$ $wR_2 = 0.2043$	$R_1 = 0.0916$ $wR_2 = 0.2028$
R indices (all data)	$R_1 = 0.1286$ $wR_2 = 0.2323$	$R_1 = 0.1831$ $wR_2 = 0.2282$
CCDC No	1036409	953195

2.6. Quantum-chemical calculations

Ab initio calculations were performed with ORCA 3.0.3 computational package at the experimental geometries determined by the X-ray diffraction for mononuclear entities [12]. The relativistic effects were included in the calculations with zero order regular approximation (ZORA) together with the scalar relativistic contracted version of TZVP basis functions.

The calculations of ZFS parameters were based on state average complete active space self-consistent field (SA-CASSCF) wave functions complemented by N-electron valence second order perturbation theory (NEVPT2) [13]. The active space of the CASSCF calculations comprised of seven electrons in five metal-based d-orbitals. The state averaged approach was used, in which all ten quartet states and forty doublets states were equally weighted. The calculations utilized the RI approximation with appropriate decontracted auxiliary basis set and the chain-of-spheres (RIJ-COSX) approximation to exact exchange. Increased integration grids (Grid4) and tight SCF convergence criteria were used. The ZFS parameters were calculated through quasi-degenerate perturbation theory in which an approximation to the Breit-Pauli form of the spin-orbit coupling operator (SOMF) and the effective Hamiltonian theory was utilized [14].

3. Results and discussion

3.1. Structural data

The structure of **3** consists of the neutral molecular units $[\text{CoCl}_2\text{L}^{\text{C10}}]$ ($Z = 4$) and three CH_3CN solvent molecules. The ligand L^{C10} is coordinated via three of its N donor atoms to the Co(II) centre and two chlorido ligands complete the coordination polyhedron of the complex.

The $\{\text{CoN}_3\text{Cl}_2\}$ chromophore possesses the Co–N bond distances from 2.065(4) to 2.155(5) Å. The Co–Cl bond distances are substantially longer, 2.285(18) and 2.269(18) Å, and the bond angle Cl–Co–Cl is 112.08(6)°. Other bond lengths as C–N, N–N and C–C in the ligand vary in the range from 1.320(7) to 1.414(7) Å, 1.375(6) to

1.360(6) Å and from 1.202(8) to 1.545(12) Å, respectively. The analysis using the SHAPE program confirms that the chromophore resembles the trigonal bipyramid (Addison geometry index $\tau = 0.35$) [15].

The structure of **5** is formed of neutral molecular units $[\text{CoCl}_2\text{-L}^{\text{C14}}]$ ($Z = 4$) and no solvent molecules are present in the crystal lattice (Fig. 1). The metal centre is coordinated by three nitrogen donor atoms from the ligand and two Cl atoms. The SHAPE analysis confirms the geometry of the tetragonal pyramid and $\tau = 0.19$. The Co–N bond distances range from 2.085(8) to 2.137(8) Å and the

average of two Co–N(amine) bonds is 2.134 Å. These bonds are longer compared to Co–N(imine) around 0.049 Å. The Co–Cl bond distances are 2.263(3) and 2.329(2) Å. The Co1–Cl2 bond length is elongated by 0.066 Å relative to the Co1–Cl1 bond distance and the bond angle Cl–Co–Cl is 111.76(10)°. Others bond lengths as C–N, N–N and C–C in the ligand vary in the range from 1.313 (11) to 1.415(11) Å, 1.361(9) to 1.400(9) Å and from 1.156(12) to 1.541(13) Å, respectively.

The key structural features of the complexes under study are summarized in Table 2. It can be seen that the mononuclear units with the geometry of the chromophore close to tetragonal pyramid (**1**, **2**, and **5**) form supramolecular dimers *via* short π – π contacts (~ 3.4 Å). Two complexes possessing the chromophore close to a trigonal bipyramid (**3** and **4**), on the contrary, form infinite chains through a partial π – π stacking of the aromatic rings (C...C ~ 3.3 Å). There is no correlation of these properties with the length of the alkyl tail of the antenna-like ligand.

The curiosity of the crystal structure of **4** lies in three aspects: (i) the crystal system is orthorhombic (Pbca) as compared to the monoclinic system (P2₁/c) for the remaining complexes; (ii) one of the cell parameters is doubled and then $Z = 8$ (instead of $Z = 4$); (iii) the chains are not packed exclusively in a parallel manner (see ESI). Remarkably, the coordination environment of **4** and **3** resembling the trigonal bipyramid ($\tau = 0.35$ and 0.41, respectively) is almost identical.

3.2. DC magnetic data

The DC magnetic measurements gave the temperature dependence of the molar magnetic susceptibility (converted to the effective magnetic moment) and the field dependence of the molar magnetization (Fig. 2). The effective magnetic moment for **3** and **5** stays almost constant on cooling from the room temperature, except the low temperature region. Below 100 K it decreases as an effect of the zero-field splitting of Co(II) centres ($|D| \gg 0$) and then it rises up owing to a kind of exchange interaction of a ferromagnetic nature ($J > 0$). Such a behaviour is analogous to that already reported for **2** [5c]. This is in contrast to the magnetic data reported for **1** and **4** where no upturn of the effective magnetic moment was observed, so that an eventual exchange interaction is either of an antiferromagnetic nature, too weak, or absent (see ESI for comparison) [9].

The DC magnetic data for **2**, **3**, and **5** (showing a ferromagnetic exchange interaction) was fitted by using an isotropic exchange model with single-ion anisotropy

$$\hat{H}_{mn} = -J(\vec{S}_1 \cdot \vec{S}_2)\hbar^{-2} + \hat{H}^z(\vartheta_m, \varphi_n) + D(\hat{S}_{Z1}^2 - \vec{S}_1^2)\hbar^{-2} + D(\hat{S}_{Z2}^2 - \vec{S}_2^2)\hbar^{-2} \quad (1)$$

Here the D-tensors were thought as collinear and the Zeeman term $\hat{H}^z(\vartheta_m, \varphi_n)$ was averaged over 120 knots distributed uniformly over one hemisphere [16]. The eigenvalues of the model Hamiltonian were inserted to the partition function from which the magnetic susceptibility and the magnetization were reconstructed by using standard formulae of the statistical thermodynamics.

The fitting procedure involves two magnetic parameters related to the single centre g_x and D ($g_z = 2.0$ has been fixed in accordance with theoretical analysis) [17], correction for the temperature-independent magnetism χ_{TIM} , and either exchange coupling constant $J > 0$ when the ferromagnetic interaction is evidenced from low-temperature susceptibility data or molecular field correction $zj < 0$ in the opposite case (**1** and **4**) in order to mimic weak intermolecular interactions [18]. No more than four parameters were optimized simultaneously in order to get a minimum of the joint error functional $F = R(\chi) \times R(M)$. The final set of magnetic param-

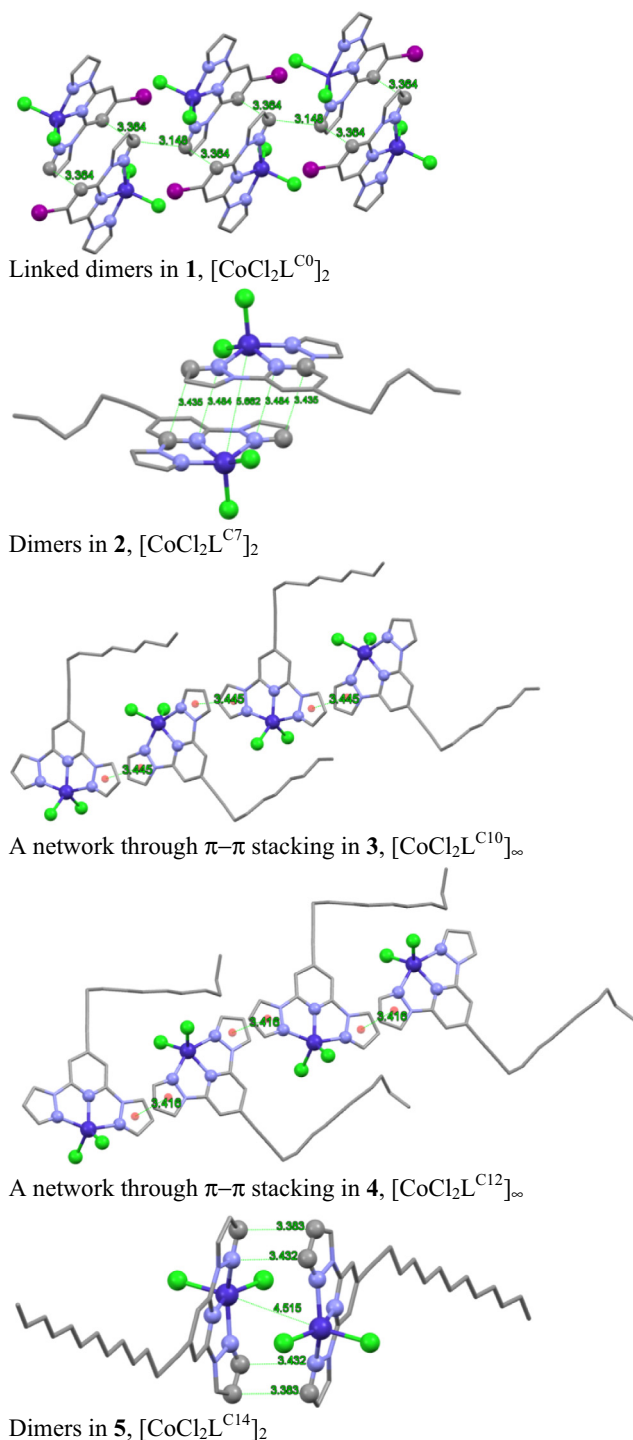


Fig. 1. Crystal packing of **1** through **5**. Eventual solvent molecules and hydrogen atoms were omitted for clarity.

Table 2
Survey of structural features for **1** through **5**.

No	Complex	SHAPE agreement factor ^a			Chrom-ophore	Principal packing	Crystal solvent
		3bpy	4py	τ			
1	[CoCl ₂ L ^{C0}] ₂	3.81	2.26	0.15	4py	Dimers	None
2	[CoCl ₂ L ^{C7}] ₂	5.17	1.90	0.01	4py	Dimers	MeCN
3	[CoCl ₂ L ^{C10}] _∞	2.83	3.46	0.35	3bpy	Chains	3MeCN
4	[CoCl ₂ L ^{C12}] _∞	2.67	4.10	0.41	3bpy	Chains	2MeCN
5	[CoCl ₂ L ^{C14}] ₂	6.95	1.88	0.19	4py	Dimers	None

^a Program SHAPE [15]. τ – Addison geometry index. 4py – tetragonal pyramid ($\tau = 0$); 3bpy – trigonal bipyramid ($\tau = 1$).

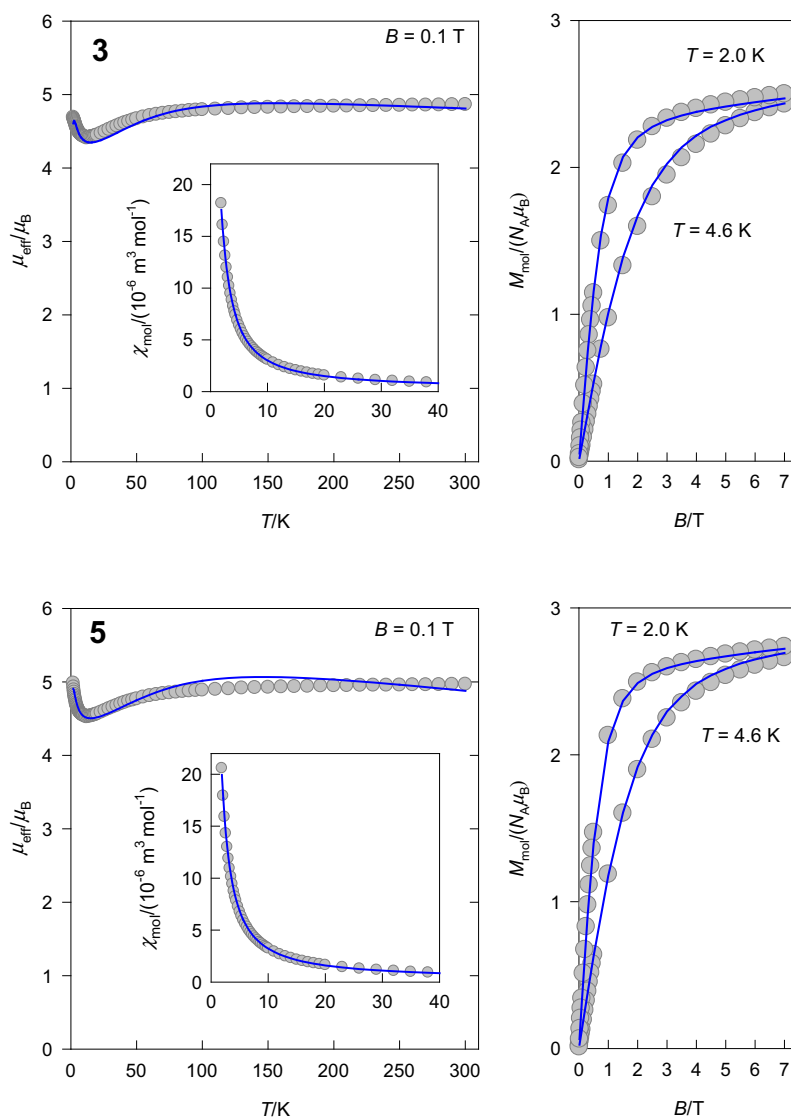


Fig. 2. Magnetic function for **3** and **5** per formula unit [CoCl₂L^{Cn}]. Left – temperature dependence of the effective magnetic moment; inset – molar magnetic susceptibility (SI units); right – field dependence of the magnetization.

eters is collected in Table 3 together with updated parameters for complexes **1**, **2**, and **4** (using a consistent model). The calculated magnetic functions are drawn as solid lines and presented per monomeric unit.

The sign and magnitude of the axial zero-field splitting parameter D for the Co(II) complexes is a long-lasting controversial story. In quasi-octahedral systems [CoL₄X₂] only the tetragonal compression matches the spin-Hamiltonian formalism as the ground crystal-field term ⁴A_{2g} is split into the ground multiplet

| S, M_S) = |3/2, ±1/2) (Γ₆) separated from the excited one | S, M_S) = |3/2, ±1/2) (Γ₇) by the gap $\Delta = 2D$ with D – positive. (In such a case $g_x \gg g_z = 2$ are predicted.) However, for an elongated tetragonal bipyramid the multiplet manifolds arise from the splitting of the ⁴E_g term and there are four Kramers doublets (Γ₆, Γ₆, Γ₇, Γ₇) that do not conform the spin-Hamiltonian formalism so that any assignment of the D value is irrelevant [19].

For quasi-tetrahedral complexes two Kramers doublets arise from the ⁴A₂ ground term and the D -parameter can adopt either

Table 3
Magnetic data for **1** through **5**.^a

No	τ	Model ^b	g_x	$D/hc/cm^{-1}$	J/cm^{-1}	$zj/hc/cm^{-1}$	χ_{TDM}^c
1	0.15	m	2.48	61.9	–	–0.059	2.5
2	0.01	d	3.03	153	1.45	–	–53
3	0.35	d	2.72	70.1	1.42	–	–18.4
4	0.41	m	2.35	46.8	–	–0.026	9.0
5	0.19	d	3.05	87.5	1.06	–	–54

^a Fixed $g_z = 2.0$.^b m – monomer, d – dimer.^c In units of $10^{-9} m^3 mol^{-1}$.

positive or negative values as confirmed by high-field/high-frequency EPR (EMR) [19].

For pentacoordinate Co(II) complexes two obstacles are in the play: (i) the geometry is usually in between ideal tetragonal pyramid (C_{4v} , 4E ground state, 4 Kramers doublets) and ideal trigonal bipyramid (D_{3h} , $^4A_1'$ ground state, two Kramers doublets); (ii) the complexes **1** through **5** are heteroleptic so that any idealization to the 4py or 3bpy geometry is problematic. The case of 4py can be modelled by removing one apical ligand (X) from a compressed tetragonal bipyramid to $[CoL_4X]$ with an increase of the bond angle X-Co-L to about 104 deg. For the 4E ground state, however, the spin-Hamiltonian formalism again is invalid and the D -parameter does not have any physical meaning. For the 4A ground state the D -parameter is positive. Moreover, for large rhombicity, when $|D| \sim 3E$, the sign of the D -parameter stays unassigned.

There is another obstacle given by the crystal packing for complexes **1** through **5**: all of them exhibit supramolecular assemblies which complicate a correct data analysis. It is difficult, if not impossible, to separate the antiferromagnetic exchange interaction and the single-ion anisotropy for $S = 3/2$ spin dinuclear system from the susceptibility data alone as shown by a modelling elsewhere [20]. However, the saturation of the magnetization is influenced only by the D -parameter (and g -components) so that a simultaneous fit of susceptibility and magnetization can catch the D parameter reliably. Best fits give for **1–5** large and positive D values. We have tested also the opposite situation, however, the fits for negative D are much worse (see Fig. S14 and Table S10 in ESI).

The experimental DC magnetic data and its analysis allow concluding that the studied systems span two groups. The first group contains **1** and **4** which can be viewed as monomers in a weak intermolecular interaction $zj < 0$. The second group containing **2**, **3**, and **5** are to be viewed as dimers with $J > 0$. DFT calculations confirm the experimental results [21].

3.3. Ab initio calculations

The magnetic parameters (axial zero-field splitting parameter D , rhombic zero-field splitting parameter E , and diagonal components of the g -tensor) were evaluated by using CASSCF/NEVPT2/QDPT method (Table 4).

Table 4
Calculated magnetic parameters (ORCA 3.0.3).

No	Geometry	Energy levels/cm ^{-1a}	Ground term	D_{calc}/cm^{-1b}	$ E/D $	g -factors
1	4py $\tau = 0.15$	0, 137, 1125, 1374, 2663, 2709	$^4E, C_{4v}$	(–61.6)	0.28	1.97, 2.33, 2.82
2	4py $\tau = 0.01$	0, 243, 574, 879, 2626, 2693	$^4E, C_{4v}$	(–119)	0.11	1.74, 1.96, 3.29
3	3bpy $\tau = 0.35$	0, 91, 1761, 2191, 2796, 3154	$^4A_2', D_{3h} (C_{3v})$	44.2	0.14	1.99, 2.37, 2.50
4	3bpy $\tau = 0.41$	0, 88, 1860, 2313, 2880, 3286	$^4A_2', D_{3h} (C_{3v})$	43.4	0.10	1.99, 2.39, 2.47
5	4py $\tau = 0.19$	0, 121, 1033, 1200, 3098, 3189	$^4E, C_{4v}$	(–58.1)	0.17	2.06, 2.32, 2.89

^a Calculated six lowest Kramers doublets (SOC corrected).^b Values in parentheses are meaningless (see main text).

Calculations confirmed the presence of large magnetic anisotropy, especially for **2**. There is a clear discrepancy in sign of the calculated D -parameters with those resulting from the magnetic data fitting: for **1**, **2**, and **5** $D_{calc} < 0$. Notice, these complexes possess the geometry of the chromophore close to the tetragonal pyramid ($\tau < 0.2$) where the ground state 4E is orbitally degenerate. In such a case the D - and E -values are meaningless. The only valuable results are energies for six lowest Kramers doublets (KDs) as listed in Table 4. Indeed, for **2** the third KD at $574 cm^{-1}$ is close lying to the second one at $243 cm^{-1}$ so that four KDs are in the play, instead of two KDs which conform the spin-Hamiltonian formalism. Moreover, the value of $g_1 = 1.74$ again contradicts the predictions of the spin-Hamiltonian formalism for d^7 systems where all $g_i > 2$ must hold true. For **3** and **4** with the geometry rather close to the trigonal bipyramid the two lowest Kramers doublets are well separated from the remaining excited ones and their energy gap is $\Delta = 2D$. These values match the values retrieved from the magnetic data fitting.

Problematic results of the ORCA calculations for a series of analogous Co(II) complexes has recently also been discussed elsewhere [22]. Unfortunately, such a big D -values prevent their determination by the high-field/high-frequency EPR at present.

Returning back to the analysis of DC magnetic data one can argue that the retrieved magnetic parameters for **1**, **2**, and **5** suffer of the same drawback: the spin Hamiltonian formalism may violate and accordingly they must be accepted with care. The negative value of the χ_{TDM} for **2**, **3** and **5** may originate in the fact that these systems show extensive intermolecular contacts so that the dimer-only model is a crude approximation.

3.4. AC magnetic data

The AC susceptibility measurements for the complexes under study are displayed in Fig. S5 (see ESI) for four frequencies of the alternating field at fixed temperature $T = 2.0 K$ where the effect of the external magnetic field to the real (in-phase) and imaginary (out-of-phase) component of the magnetic susceptibility is mapped. At the zero field the out-of-phase component χ'' is almost zero but with increasing B_{DC} it rises progressively to a maximum between 0.1 and 0.2 T (depending upon the frequency f of the AC field). This confirms that the SMM behaviour of the studied com-

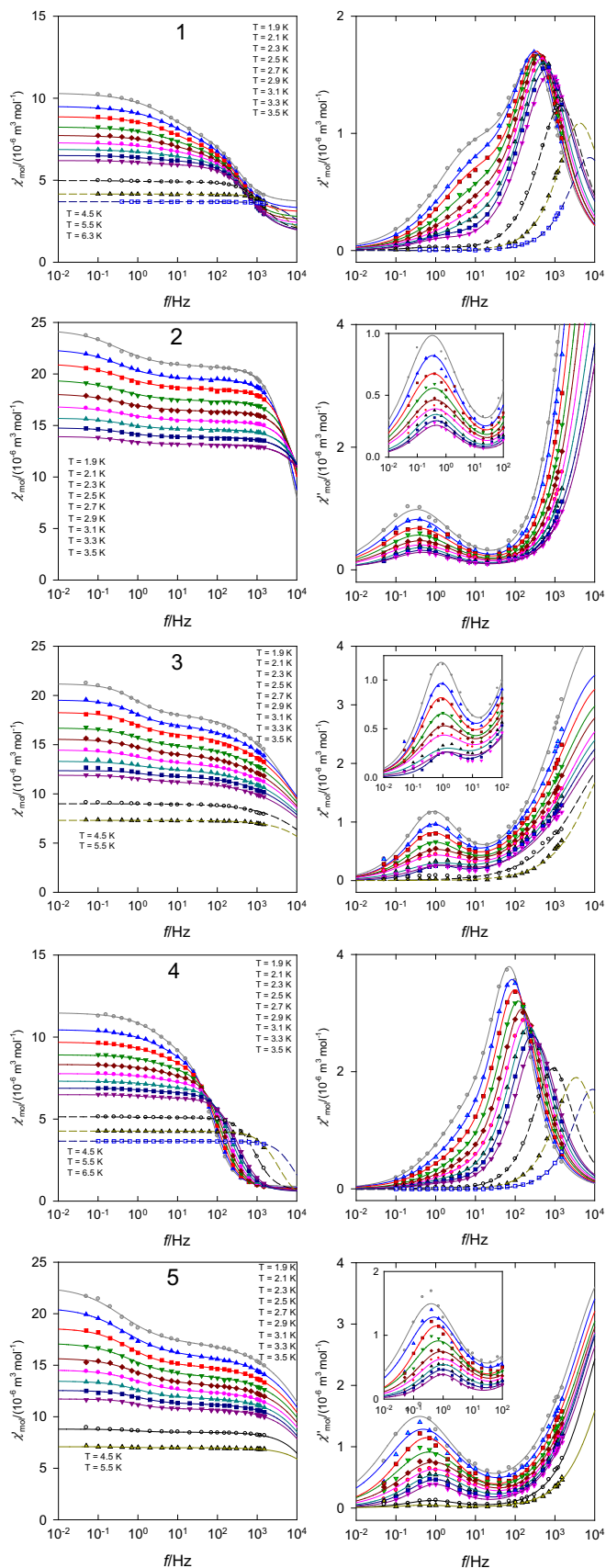


Fig. 3. Frequency dependence of the AC susceptibility components for **1** through **5** at $B_{DC} = 0.2$ T. Solid lines – fitted to the generalized Debye model with two relaxation branches.

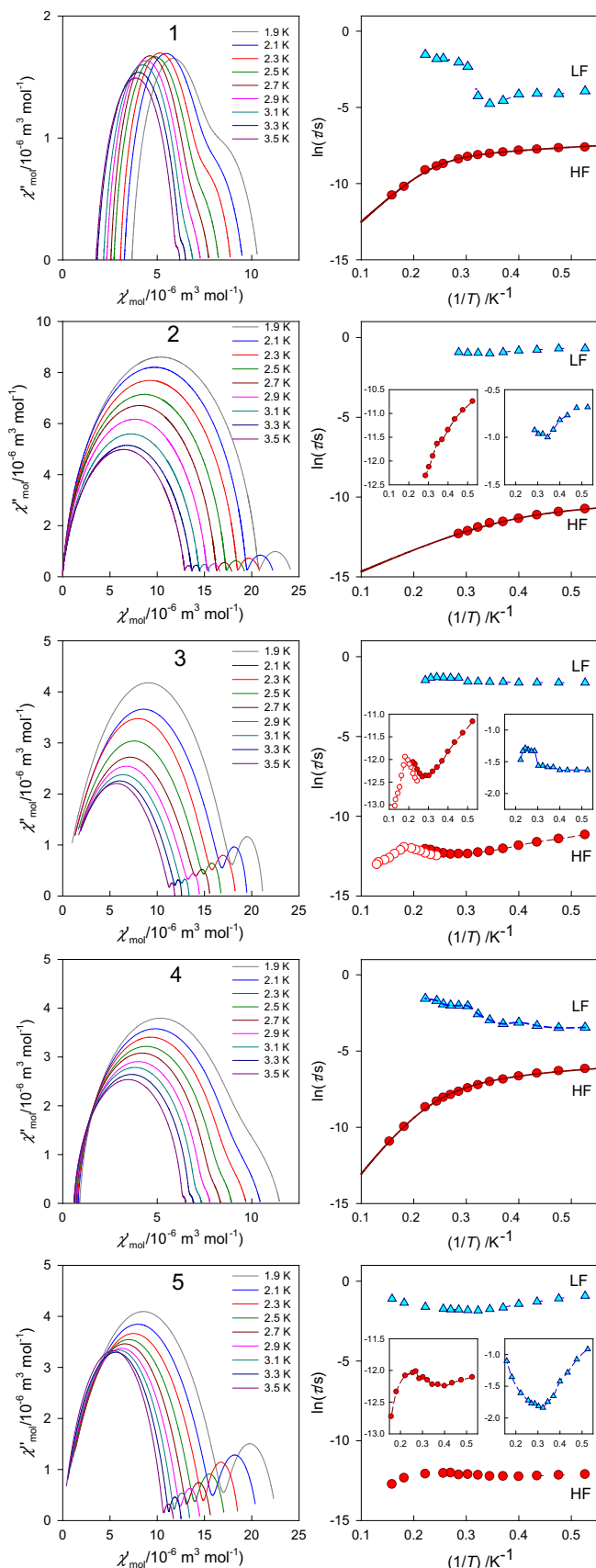


Fig. 4. The AC susceptibility data for **1** through **5** at $B_{DC} = 0.2$ T. Left – Argand plot; lines based upon fitted parameters. Right – Arrhenius-like plot with solid lines based upon fits to Eq. (4) and dashed as a guide for eyes.

plexes depends upon the applied field. The subsequent AC measurements were done at $B_{DC} = 0.2$ T, respectively.

The AC susceptibility data for **1** through **5** are displayed in Fig. 3 as functions of the frequency of the alternating field. In complexes **2**, **3**, and **5** a slow relaxation process is evident around $f \sim 1$ Hz and the corresponding peaks in the χ'' vs f plot tend to disappear on temperature increase (low-frequency, LF branch). At the same time an onset of the second peak is visible though its maximum lies outside the limits of the applied hardware; this refers to a faster relaxation process (high-frequency, HF branch).

For the complexes **1** and **4** well defined maxima around $f = 10^2$ – 10^3 Hz are seen on χ'' . However there is a low-frequency shoulder at $f \sim 10$ Hz and a correct fit is obtained only by considering two relaxation processes. (Notice, for these complexes the ferromagnetic exchange coupling was not detected.)

An extended Debye model has been used in interpreting the frequency dependence of the AC magnetic susceptibility in the form

$$\widehat{\chi}(\omega) = \chi_s + (\chi_{T1} - \chi_s) / [1 + (i\omega\tau_1)^{1-\alpha_1}] + (\chi_{T2} - \chi_{T1}) / [1 + (i\omega\tau_2)^{1-\alpha_2}] \quad (2)$$

where, two relaxation times (τ_1 , τ_2) and two distribution parameters (α_1 , α_2) occur along with two isothermal susceptibilities (χ_{T1} , χ_{T2}) and a common adiabatic susceptibility (χ_s); $\omega = 2\pi f$. This equation is decomposed into two components as shown in ESI. The fitting procedure has been based upon minimization of a joint functional $F = w\chi''(\omega) + (1-w)\chi''(\omega)$ that accounts to both susceptibility components (typical weight is $w = 0.07$). The results in the numerical form are listed in ESI.

The out-of-phase susceptibility has been plotted versus the in-phase component and in this way the Argand (Cole–Cole) diagram has been constructed – Fig. 4. Two distorted semicircles are heavily overlapped (on the left) and since not always the maxima are well visible, two primitive curves were utilized in generating Arrhenius-like plot (on the right). The two relaxation processes on heating behave differently. For the faster (HF) branch the relaxation time τ_2 decreases with temperature and this behaviour is detected for **1** through **5**. This is a usual situation found in related mononuclear and polynuclear systems. We are assigning this branch to relaxation of mononuclear entities, i.e. $[\text{CoCl}_2\text{L}^{\text{Cn}}]$ units. The slower (LF) branch exhibits a more complex behaviour specific for individual complex under study. Notice, the peak on χ'' referring to this

relaxation branch disappears progressively on heating, and the fitting procedure yields the corresponding τ -value with increasing standard error; above some temperature limit (>3.5 K) the peak is hardly resolved and above 5 K it cannot be processed by the fitting procedure.

The similarity of **1** and **4** is evident also from the LF relaxation branch: on heating the value of τ_1 decreases but then tends to increase. This is a very delicate finding than cannot be answered at the present stage. This effect might be attributed to a small structural change at the communication channel caused by temperature, i.e. it could be assigned to the more, or less perfect alignment of the aromatic rings transmitting the exchange interaction between the mononuclear units forming either $[\text{CoCl}_2\text{L}^{\text{CO}}]_2$ or $[\text{CoCl}_2\text{L}^{\text{C12}}]_{\infty}$ supramolecular assemblies. In these systems the exchange interaction is not of the ferromagnetic nature ($|J| > 0$ holds true). The non-zero adiabatic susceptibility χ_s occurs in these two systems.

The natural logarithm of the relaxation time is expected to follow a linear relationship for a thermal activation process

$$\ln(1/2\pi f_{\text{max}}^n) = \ln\tau_0 + (U/k_B)/T \quad (3)$$

The situation is more complex since in addition to the Orbach (thermal) process also the Raman and direct processes are in the play [3]. Therefore the faster relaxation time (characterized by τ_2) has been fitted by using the formula

$$\tau^{-1} = \tau_0^{-1} \exp(-U/k_B T) = +AB^m T + CT^n \quad (4)$$

where the Orbach process (U , τ_0), direct process (parameters A , m), and Raman process (parameters C , n) are accounted for. The parameters of the SMM behaviour are listed in Table 5. It can be seen that the faster (HF) relaxation branch displays characteristics that are typical for other SMM based upon mononuclear Co(II) [1]. However, the LF relaxation branch is much slower: τ (LF, 1.9 K) ~ 0.5 s for **2** and **5**.

The possible mechanism of the spin relaxation of easy plane systems based on mononuclear Co(II) complexes with large magnetic anisotropy has been proposed by considering the nuclear spin $I(\text{Co}) = 7/2$ [23]. According to this analysis, a direct term that includes the hyperfine interaction dominates at low temperatures and a Raman term is predominant for temperatures above 4 K.

Table 6 serves for the comparison of structural and magnetic parameters of **1** through **5**. The most imperative is the question

Table 5
Parameters of the SMM behaviour for **1** through **5**.

No	Branch	τ (1.9 K)/s	$U/k_B/K^{-1}$	τ_0/s	$A/T^{-m} K^{-1} s^{-1} m = 2$	$C/K^{-n} s^{-1} n = 5$
1	LF	19.7×10^{-3}	31.3(10)	$1.69(28) \times 10^{-7}$	$2.53(16) \times 10^4$	–
	HF	0.50×10^{-3}				
2	LF	494×10^{-3}	14.6(20)	$1.07(55) \times 10^{-7}$	$56.1(74) \times 10^4$	–
	HF	21.7×10^{-6}				
3	LF	193×10^{-3}	40.5(19)	$5.96(10) \times 10^{-8}$	$0.59(12) \times 10^4$	1.8(4)
	HF	14.2×10^{-6}				
4	LF	31.9×10^{-3}	40.5(19)	$5.96(10) \times 10^{-8}$	$0.59(12) \times 10^4$	1.8(4)
	HF	2.12×10^{-3}				
5	LF	450×10^{-3}	40.5(19)	$5.96(10) \times 10^{-8}$	$0.59(12) \times 10^4$	1.8(4)
	HF	4.67×10^{-6}				

Table 6
Comparison of key characteristics of **1** through **5**.^a

No	Chromo-phore	Assembly	Exchange	(LF)-(HF) overlap	Position of $f_{\text{max}}^{\text{HF}}$ /Hz @ 1.9 K	χ_s
1	4py	Dimers	$J \sim 0$	Yes	323	>0
2	4py	Dimers	$J > 0$	No	>1500	Fixed to 0
3	3bpy	Chains	$J > 0$	No	>1500	Fixed to 0
4	3bpy	Chains	$J \sim 0$	Yes	76	>0
5	4py	Dimers	$J > 0$	No	>1500	Fixed to 0

^a (LF) – slower, low-frequency relaxation branch, (HF) – faster, high-frequency relaxation branch.

about the structural predispositions of **3** and **4** leading to different DC and AC magnetic behaviour. This can originate in the different space group, and the crystal packing of the chains with aliphatic tails organized either parallel or in a strongly angled manner (consult Fig. S2 of ESI).

4. Conclusions

Using advanced chemical synthesis new tridentate ligands of the antenna-type L^{Cn} (with $n = 0, 7, 10, 12$, and 14) have been isolated and used in complexation reactions with Co(II) salts. Five mononuclear complexes of the $[CoCl_2L^{Cn}]$ type were synthesized and structurally characterized. All of them show a supramolecular assembly: **1**, **2** and **5** are dimers $[CoCl_2L^{Cn}]_2$, in which the mononuclear entities resemble a tetragonal pyramid. On the contrary, **3** and **4** form chains held by the π - π stacking of the aromatic rings and their mononuclear constituents refer to the trigonal bipyramid. The DC magnetic measurements confirm a substantial magnetic anisotropy expressed by the axial zero-field splitting parameter D . The data fitting is successful only when an exchange interaction of the ferromagnetic nature is considered for **2**, **3** and **5**.

The AC susceptibility measurements, all conducted at the external magnetic field $B_{DC} = 0.2$ T, show an existence of two relaxation branches for all five compounds. For the low-frequency branch the peak of the out-of-phase susceptibility exists at $f = 1$ – 10 Hz which determines magnetic relaxation as slow as $\tau \sim 0.5$ s at $T = 1.9$ K. This peak escapes rapidly on heating and its thermal development results in a complex behaviour of the corresponding relaxation time. Quantitatively **1** and **4** behave analogously one another as the low-frequency peak appears as a shoulder of the high-frequency peak (no ferromagnetic exchange was evidenced for these two compounds). On the contrary, **2**, **3** and **5** with $J > 0$ display the LF and the onset of the HF peaks well separated. The relaxation time adopts values typical for mononuclear Co(II) complexes ($\tau = 10^{-6}$ s at $T = 1.9$ K). The curved Arrhenius-like plot referring to the HF branch can be fitted by the extended model in which, in addition to the Orbach process, also the direct and eventually Raman processes are considered. In this way the extrapolated relaxation time for the pure thermally activated (Orbach) process adopts values of $\tau_0 \sim 10^{-7}$ s.

Acknowledgments

Slovak grant agencies (VEGA 1/0534/16, APVV-14-0078) are acknowledged for the financial support. We thank the KIT-INT staff and Dr. P. N. Martinho for their support during synthesis and measurements.

Appendix A. Supplementary data

CCDC 1036409 and 953195 contains the supplementary crystallographic data for this paper. These data can be obtained free of charge via <http://www.ccdc.cam.ac.uk/conts/retrieving.html>, or from the Cambridge Crystallographic Data Centre, 12 Union Road, Cambridge CB2 1EZ, UK; fax: (+44) 1223-336-033; or e-mail: deposit@ccdc.cam.ac.uk. Supplementary data associated with this article can be found, in the online version, at <http://dx.doi.org/10.1016/j.poly.2017.01.028>.

References

- [1] (a) G.A. Craig, M. Murrie, *Chem. Soc. Rev.* **44** (2015) 2135; (b) S. Gomez-Coca, D. Aravena, R. Morales, E. Ruiz, *Coord. Chem. Rev.* **289–290** (2015) 379; (c) J.M. Frost, K.L.M. Harriman, M. Murugesu, *Chem. Sci.* **7** (2016) 2470.
- [2] L. Chen, J. Wang, J.-M. Wei, W. Wernsdorfer, X.-T. Chen, Y.-Q. Zhang, Y. Song, Z.-L. Xue, *J. Am. Chem. Soc.* **134** (2012) 15704.
- [3] (a) X.-C. Huang, C. Zhou, D. Shao, X.-Y. Wang, *Inorg. Chem.* **53** (2014) 12671; (b) F. Habib, I. Korobkov, M. Murugesu, *Dalton Trans.* **44** (2015) 6368; (c) D. Shao, S.-L. Zhang, L. Shi, Y.-Q. Zhang, X.-Y. Wang, *Inorg. Chem.* **55** (2016) 10859; (d) D. Shao, L. Shi, S.-L. Zhang, X.-H. Zhao, D.-Q. Wu, X.-Q. Wei, X.-Y. Wang, *Cryst. Eng. Commun.* **18** (2016) 4150; (e) P. Antal, B. Drahoš, R. Herchel, Z. Trávníček, *Inorg. Chem.* **55** (2016) 5957.
- [4] (a) J. Vallejo, I. Castro, J. Ruiz-Garcia, J. Cano, M. Julve, F. Lloret, G. De Munno, W. Wernsdorfer, E. Pardo, *J. Am. Chem. Soc.* **134** (2012) 15704; (b) E. Colacio, K. Ruiz, E. Ruiz, E. Cremades, J. Krzystek, S. Carretta, J. Cano, T. Guidi, W. Wernsdorfer, E.K. Brechin, *Angew. Chem. Int. Ed.* **52** (2013) 9130; (c) Y.-Y. Zhu, C. Cui, Y.-Q. Zhang, J.-H. Jia, X. Guo, C. Gao, K. Qian, S.-D. Jiang, B.-W. Wang, Z.-M. Wang, S. Gao, *Chem. Sci.* **4** (2013) 1802; (d) I.A. Gass, S. Tewary, A. Nafady, N.F. Chilton, C.J. Gartshore, M. Asadi, D.W. Lupton, B. Moubarakí, A.M. Bond, J.F. Boas, S.-X. Guo, G. Rajaraman, K.S. Murray, *Inorg. Chem.* **52** (2013) 7557; (e) M.S. Fataftah, J.M. Zadrozny, D.M. Rogers, D.E. Freedman, *Inorg. Chem.* **53** (2014) 10716; (f) R. Herchel, L. Váhovská, I. Potočník, Z. Trávníček, *Inorg. Chem.* **53** (2014) 5896.
- [5] (a) F. Habib, O.R. Luca, V. Vieru, M. Shiddiq, I. Korobkov, S.I. Gorelsky, M.K. Takase, L.F. Chibotaru, S. Hill, R.H. Crabtree, M. Murugesu, *Angew. Chem. Int. Ed.* **52** (2013) 11290; (b) T. Jurca, A. Farghal, P.-H. Lin, I. Korobkov, M. Murugesu, D.S. Richeson, *J. Am. Chem. Soc.* **133** (2011) 15814; (c) C. Rajnák, J. Titiš, O. Fuhr, M. Ruben, R. Boča, *Inorg. Chem.* **53** (2014) 8200; (d) R. Ruamps, L.-J. Batchelor, R. Guillot, G. Zakhia, A.-L. Barra, W. Wernsdorfer, N. Guihéry, T. Mallah, *Chem. Sci.* **5** (2014) 3418; (e) I. Nemeč, R. Marx, R. Herchel, P. Neugebauer, J. van Slageren, Z. Trávníček, *Dalton Trans.* **44** (2015) 15014; (f) A. Packová, J. Miklovič, R. Boča, *Polyhedron* **102** (2015) 88.
- [6] (a) W. Huang, T. Liu, D. Wu, J. Cheng, Z.W. Ouyang, C. Duan, *Dalton Trans.* **42** (2013) 15326; (b) F. Yang, Q. Zhou, Y. Zhang, G. Zeng, G. Li, Z. Shi, B. Wang, S. Feng, *Chem. Commun.* **49** (2013) 5289; (c) R. Boča, J. Miklovič, J. Titiš, *Inorg. Chem.* **53** (2014) 2367; (d) M.R. Saber, K.R. Dunbar, *Chem. Commun.* **50** (2014) 12266; (e) J.M. Zadrozny, J. Liu, N.A. Piro, C.J. Chang, S. Hill, J.R. Long, *Chem. Commun.* **48** (2012) 3927; (f) J.M. Zadrozny, J.R. Long, *J. Am. Chem. Soc.* **133** (2011) 20732; (g) J.M. Zadrozny, J. Telsner, J.R. Long, *Polyhedron* **64** (2013) 209; (h) L. Smolko, J. Černák, J. Dušek, J. Miklovič, J. Titiš, R. Boča, *Dalton Trans.* **44** (2015) 17565; (i) C. Rajnák, A. Packová, J. Titiš, J. Miklovič, J. Moncol', R. Boča, *Polyhedron* **110** (2016) 85.
- [7] A. Eichhofer, Y. Lan, V. Mereacre, T. Bodenstein, F. Weigend, *Inorg. Chem.* **53** (2014) 1962.
- [8] (a) R.L. Carlin, *Magnetochemistry*, Springer, Berlin, 1986, p. 49; (b) R.L. Carlin, R.D. Chirico, E. Sinn, G. Mennenga, L.J. de Jongh, *Inorg. Chem.* **21** (1982) 2218; (c) J.M. Zadrozny, M. Atanasov, A.M. Bryan, C.-Y. Lin, B.D. Rekker, P.P. Power, F. Neese, J.R. Long, *Chem. Sci.* **4** (2013) 125.
- [9] C. Rajnák, J. Titiš, I. Šalitroš, R. Boča, O. Fuhr, M. Ruben, *Polyhedron* **65** (2013) 122.
- [10] (a) C. Rajadurai, Z. Qu, O. Fuhr, Z. Gopalan, R. Kruk, M. Ghafari, M. Ruben, *Dalton Trans.* **32** (2007) 3531; (b) C. Rajadurai, F. Schramm, O. Fuhr, M. Ruben, *Eur. J. Inorg. Chem.* **17** (2008) 2649; (c) C. Rajadurai, O. Fuhr, R. Kruk, M. Ghafari, M. Hahn, M. Ruben, *Chem. Commun.* **25** (2007) 2636; (d) N.T. Madhu, I. Šalitroš, F. Schramm, S. Klyatskaya, O. Fuhr, M. Ruben, C. R. Chim. **11** (2008) 1166; (e) I. Šalitroš, J. Pavlik, R. Boča, O. Fuhr, C. Rajadurai, M. Ruben, *Cryst. Eng. Commun.* **12** (2010) 2361.
- [11] G.M. Sheldrick, *Acta Cryst.* **A64** (2008) 112.
- [12] F. Neese, The ORCA program system, *Wiley Interdiscip. Rev. Comput. Mol. Sci.* **2** (2012) 73.
- [13] (a) F. Neese, ORCA – An Ab Initio, Density Functional and Semi-empirical Program Package, Version 3.0.3.; (b) M. Atanasov, D. Ganyushin, D.A. Pantazis, K. Sivalingam, F. Neese, *Inorg. Chem.* **50** (2011) 7460; (c) C. Angeli, S. Borini, M. Cestari, R.J. Cimiraglia, *Chem. Phys.* **121** (2004) 4043; (d) C. Angeli, R. Cimiraglia, S. Evangelisti, T. Leininger, J.-P. Malrieu, *J. Chem. Phys.* **114** (2001) 10252; (e) C. Angeli, R. Cimiraglia, J.-P. Malrieu, *J. Chem. Phys.* **117** (2002) 9138.
- [14] (a) F. Neese, *J. Chem. Phys.* **122** (2005) 34107; (b) D. Ganyushin, F. Neese, *J. Chem. Phys.* **125** (2006) 24103; (c) F. Neese, *J. Chem. Phys.* **127** (2007) 164112.
- [15] M. Llunell, D. Casanova, J. Cirera, P. Alemany, S. Alvarez, Program SHAPE, Ver. 2.1. University of Barcelona. Note: the program assumes a spherical distribution of the ligands in ideal reference polygons or polyhedra, 2013.
- [16] J. Hudák, R. Boča, J. Moncol', J. Titiš, *Inorg. Chim. Acta* **394** (2013) 401.
- [17] R. Boča, *Struct. Bond.* **117** (2006) 1.
- [18] B. Papánková, R. Boča, L. Dlháň, I. Nemeč, J. Titiš, I. Svoboda, H. Fuess, *Inorg. Chim. Acta* **363** (2010) 147.
- [19] M. Idešicová, J. Titiš, J. Krzystek, R. Boča, *Inorg. Chem.* **52** (2015) 9409.

- [20] (a) R. Boča, *Theoretical Foundations of Molecular Magnetism*, Elsevier, Amsterdam, 1999;
(b) R. Boča, *A Handbook of Magnetochemical Formulae*, Elsevier, Amsterdam, 2012.
- [21] Magnetic coupling between the molecules has been confirmed by density functional theory (DFT) calculations. The dimeric units in its experimental geometry have been calculated by the ORCA program using the TZVP basis set for all elements and the appropriate set of auxiliary functions. B3LYP (RIJCOSX) calculations with the broken-symmetry approach gave J/hc (cm^{-1}) (Yamaguchi formula): -0.60 (1), 0.54 (2), 1.57 (3), -0.28 (4), 0.78 (5).
- [22] I. Nemeč, H. Liu, R. Herchel, X. Zhang, Z. Trávníček, *Synth. Met.* **215** (2016) 158.
- [23] S. Gómez-Coca, A. Urtizberea, E. Cremades, P.J. Alonso, A. Camón, E. Ruiz, F. Luis, *Nat. Commun.* **5** (2014) 4300.